

Modular Dual Active Bridge converter architecture

Pablo Zumel⁽¹⁾, Leonardo Ortega⁽³⁾, Antonio Lázaro⁽¹⁾, Cristina. Fernández⁽¹⁾, Andres Barrado⁽¹⁾, Alberto Rodríguez⁽²⁾, Marta María Hernando⁽²⁾

⁽¹⁾ Carlos III University of Madrid, Power Electronics Systems Group (GSEP)
Av. Universidad 30, 28911 Leganes, Spain
e-mail: pzumel@ing.uc3m.es

⁽²⁾ University of Oviedo. Electronic Power Supply Systems Group (SEA).
Campus de Viesques 33204, Gijón. Spain
e-mail: rodriguezalberto@uniovi.es

⁽³⁾ Escuela Politécnica Nacional
Ladrón de Guevara E11 - 253.
Quito, Ecuador
e-mail: leonardo.ortega@epn.edu.ec

Abstract— This paper describes a modular¹ architecture based on the Dual Active Bridge (DAB) converter in input series, output parallel (ISOP) connection. The work is focused on the input voltage sharing to ensure a proper operation of each module by means of an active control of input and output voltages. A small signal model of the modular architecture is proposed and a decoupled control loops scheme is used to implement the control strategy. An experimental setup has been built in order to validate the model of the DAB converter in ISOP connection and the proposed control strategy, taking into account different operating conditions and constructive parameter values.

I. INTRODUCTION

Modular or multi-cell approach is being explored in the last years [1]-[7] as an alternative to increase the voltage and current levels handled by the power converters, increasing efficiency, reducing cost and enhancing output performance like output ripple [1]. The combination of series connection of the input ports and parallel connection of the output ports of the converter (Input Series-Output Parallel, ISOP) [2][4][5][6][8], enables high input voltage and high output current converters with optimized operation. Besides the technical advantages, the use of standard conversion cells to build different power converters for a wide range of specifications can lead to cost reduction by the effect of scale economies.

Control in modular architectures becomes a key issue, since a proper voltage and current distribution among the modules must be ensured to achieve a safe and good operation [2][4][7][8]. In the case of ISOP connection, the input voltage and output current of each module must be kept within an acceptable range, being the ideal the same values for all the modules. Output voltage must be also regulated. Previous works have addressed the problem of control in ISOP configurations using different approaches. In [2] a combination of voltage and current loops is used to distribute input voltages in two modules; in [4] a charge control with an input voltage

feedforward is used to control two full-bridge converters sharing an input filter; in [7] a common duty ratio control is used to ensure equalized operation, averaging the control signal of different control loops; in [8] a decoupling technique to control independently many ISOP full-bridge modules is proposed.

One of the topologies that can be suitable for a modular approach is the Dual Active Bridge (DAB) [9]-[26], especially for high voltage applications. The DAB converter has been used in high power [9][10][16][20][23][24][25] and medium power [11][12][13][14][15][17][21][26] applications. The DAB converter (Figure 1), is a bidirectional DC/DC converter based on two active bridges interfaced through a high-frequency transformer (with a great influence of its leakage inductance), enabling power flow in both directions in case of active load. The simplest way to control this topology is switching each full bridge with a constant duty cycle of 50% to generate a high-frequency square-wave voltage at its transformer terminals ($\pm v_{in}$, $\pm v_o$) [21][22]. Considering the presence of the leakage inductance of the transformer (with a controlled and known value), the two square waveforms can be properly phase-shifted. These two phase-shifted signals (v_1 and v_2) generate a voltage (v_{Lk}) across the leakage inductance (L_k) of the transformer and a certain current (i_{Lk}) flowing through it (Figure 1). This current is controlled by the phase-shift between the primary and secondary voltages of the transformer (v_1 and v_2). The sign of the phase-shift controls the direction of the power flow from one pair of terminals to the other, and bidirectional power transfer can be achieved. Power is delivered from the bridge which generates the leading square wave.

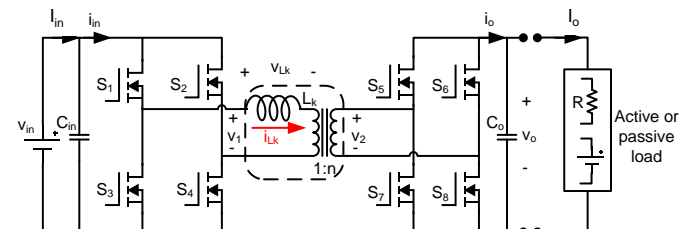


Figure 1 Schematic of the DAB converter

¹ Part of this paper has been presented at the 2014 IEEE Applied Power Electronics Conference and Exposition, Fort Worth TX 16-20 March 2014

This work is focused on the analysis of the ISOP connection of three DAB converters (Figure 2). The goal is the design of a control strategy to ensure a proper distribution of input voltages, despite differences in the constructive parameters of the modules, applying a decoupling technique [8]. The main contributions of this work are the small signal model of the DAB modular converter, the application of a decoupling technique and the experimental validation of the control strategy.

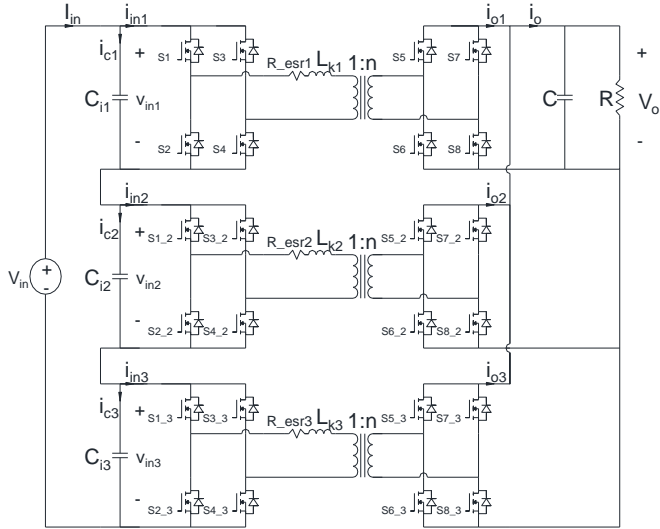


Figure 2 DAB converters in input series output parallel connection

The paper is organized as follows: in section II the steady state operation of the DAB converter is reviewed and the problem of the ISOP connection is introduced; in section III the small signal model of the modular DAB architecture is presented and the decoupled loops technique is applied to the model; in section IV experimental results are reported: steady state characterizations of the modular DAB architecture, small signal model verification and control strategy validation.

II. STEADY STATE CHARACTERIZATION

The basics operation principles and the key waveforms of the DAB converter have been presented in [22]. In the analysis presented in this reference, the DAB is controlled using the Phase-Shift Modulation (PSM) strategy. As the inductor voltage evokes the typical waveform of conventional PWM converters, the control parameter will be called duty cycle “d”. One of the major advantages of the DAB is the soft switching operation of all the devices at nominal conditions. However, when the power handled by the DAB is reduced, ZVS can be lost. When $V_{in}=V_o/n$, ZVS is theoretically obtained in all the operation range. Nevertheless, when $V_{in}\neq V_o/n$, ZVS is not obtained in all the power range. Other possibilities different from PSM to control the DAB converter has been studied in other works [13]-[19] to improve ZVS range, light load behavior, etc.

The average model of the converter can be represented by two current sources (Figure 3), one for the input current and another one for the output current. The equations of the average model of an ideal DAB converter (1), (2) and (3) were presented in [22], where I_o is the output average current, I_{in} is the input average current (see Figure 1), T is half the switching period, D (duty cycle) is the normalized phase-shift between the switching signals of the input and the output bridges ([22]), n is the transformer turns ratio, L_k is the transformer leakage inductance, V_o is the average output voltage, V_{in} is the input voltage and R is the load resistance. Resistive load is considered in (3).

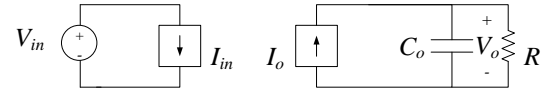


Figure 3 Steady state model of a DAB converter

$$I_o = \frac{T \cdot V_{in} \cdot D \cdot (1 - D)}{L_k \cdot n} \quad (1)$$

$$I_{in} = \frac{T \cdot V_o \cdot D \cdot (1 - D)}{L_k \cdot n} \quad (2)$$

$$V_o = \frac{T \cdot V_{in} \cdot D \cdot (1 - D)}{L_k \cdot n} R \quad (3)$$

Equation (2) indicates that the output voltage and the input current of a DAB are related by T , D , L_k and n . However, in an ISOP connection all the modules have identical output voltage and input current (Figure 2), so if the modules are not exactly identical and operating with the same D and T , there will be a difference between the total input current (I_{in} in Figure 2), defined by the connection of the modules, and the input current of each module (i_{in1} , i_{in2} , i_{in3}). The current through the input capacitors will not be zero, starting a runaway process where only one module supports all the input voltage.

In practice, even though those parameters are not equal, there is a proper steady state operation point, since the converters do not behave exactly like ideal current sources, but there is an equivalent output impedance. The distribution of the power processed by the different modules depends on the parasitic values of each converter, as in other multiconverter structures, e.g. interleaved multiphase converters.

In a DAB modular converter there are two main advantages of achieving a uniform distribution of the input voltage among the modules (input voltage sharing). On one hand, the power processed by the different modules must be almost the same, in order to avoid oversizing the modules. On the other hand, ZVS must be ensured in many applications. As it has been previously said, the input voltage of each module can determine the achievement of ZVS, and a uniform distribution

of voltage ensures a wide operation range of all modules under soft switching conditions. Even if an unequal input voltage distribution were acceptable, it may yield a ZVS loss in some modules, as it is shown in Figure 4, where three DAB converters in ISOP connection have been simulated with different values of the inductance L_k . In Figure 4 (upper plot) the difference among the inductance values is $\pm 0.16\%$ and it generates a difference in the input voltage of 1%, having the same ZVS behavior for the three modules. In case of a difference of $\pm 1.6\%$, differences among input voltages are around 10%, which can be an acceptable value. However, Figure 4 (lower plot) shows that ZVS is lost for one of the modules, with a deep impact over the system efficiency.

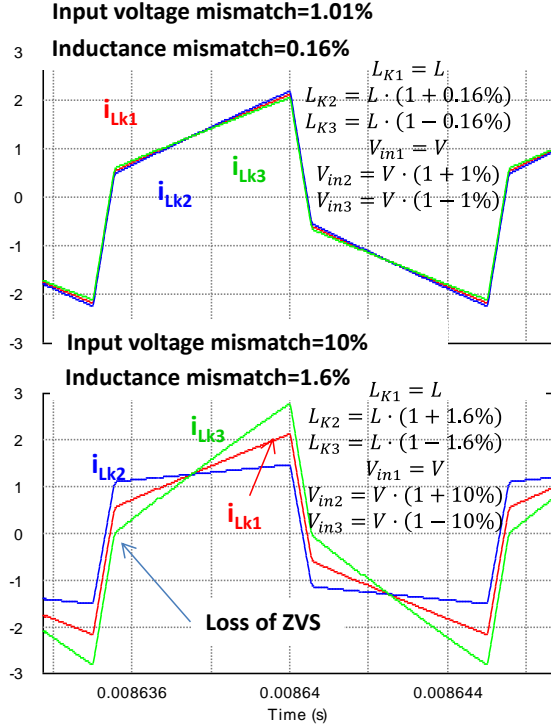


Figure 4. Inductor current waveforms in a system with 3 DAB converters in ISOP connection considering two different values for the inductance mismatch

III. DYNAMIC MODELING AND DECOUPLED CONTROL LOOPS

Taking as starting point the average model of the DAB converter (1) and (2), the equations corresponding to the small signal model are (4) and (5) [21].

As one of the advantages of DAB converters is bidirectionality, two operation modes can be considered: 1) *forward operation mode*, where power goes from the side of series connected ports to the side of paralleled ports; 2) *reverse operation mode*, where power goes from paralleled ports to the side of series connected ports.

The dynamics are different in case of an ideal voltage source when compared to the resistive load. However, although resistive load is assumed, the model and control strategy can be also applied when the load is not an ideal voltage source, but a voltage source with a series resistance, like a battery [22]. In this case the dynamics is determined by the series resistance of the voltage source.

$$\hat{i}_o = g_{ovi} \cdot \hat{v}_{in} + g_{od} \cdot \hat{d} \quad (4)$$

$$g_{ovi} = \frac{V_o}{V_{in} \cdot R}; \quad g_{od} = \frac{V_o \cdot (1 - 2D)}{(1 - D) \cdot D \cdot R}$$

$$\hat{i}_{in} = g_{ivo} \cdot \hat{v}_o + g_{id} \cdot \hat{d}; \quad (5)$$

$$g_{ivo} = \frac{V_o}{V_{in} \cdot R}; \quad g_{id} = \frac{V_o}{V_{in}} g_{od}$$

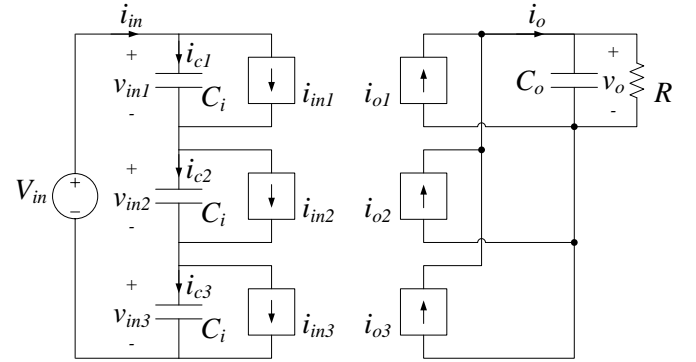


Figure 5 Average model circuit for DAB in ISOP connection.

A. Small signal model of DAB in ISOP connection (forward operation)

The small signal model of the DAB converters in ISOP connection is based on the small signal computations over the averaged model of Figure 5. The assumptions considered for this model are the following [27]:

- All the modules have the same values of L_k , n , T , and input capacitors ($C_{i1} = C_{i2} = C_{i3} = C_i$).
- All the modules have a DC average value equal to 1/3 of the input voltage ($V_{in1} = V_{in2} = V_{in3} = \frac{V_{in}}{3}$);
- All the modules have exactly the same duty cycle ($D_1 = D_2 = D_3 = D$) in the operating point, though different perturbations ($\hat{d}_1 \neq \hat{d}_2 \neq \hat{d}_3$) are considered.

The main equations of this model are summarized in (6) and (7), where the perturbation of the input voltage of a given module and the perturbation of the output voltage are obtained from the perturbations of the duty cycle of each module, respectively. Coefficients g_{od} and g_{id} are calculated from expressions (4) and (5), where V_{in} is the total input voltage and V_o is the output voltage.

$$\hat{v}_{inj} = \frac{1}{C_i \cdot s} \cdot g_{id} \cdot \left(\frac{1}{3} \cdot (\hat{d}_1 + \hat{d}_2 + \hat{d}_3) - \hat{d}_j \right) \quad (6)$$

$$\begin{aligned} \hat{v}_o &= \frac{R}{RC_o s + 1} \cdot \frac{g_{od}}{3} \cdot (\hat{d}_1 + \hat{d}_2 + \hat{d}_3) \\ &= G_{vd}(s) \cdot (\hat{d}_1 + \hat{d}_2 + \hat{d}_3) \end{aligned} \quad (7)$$

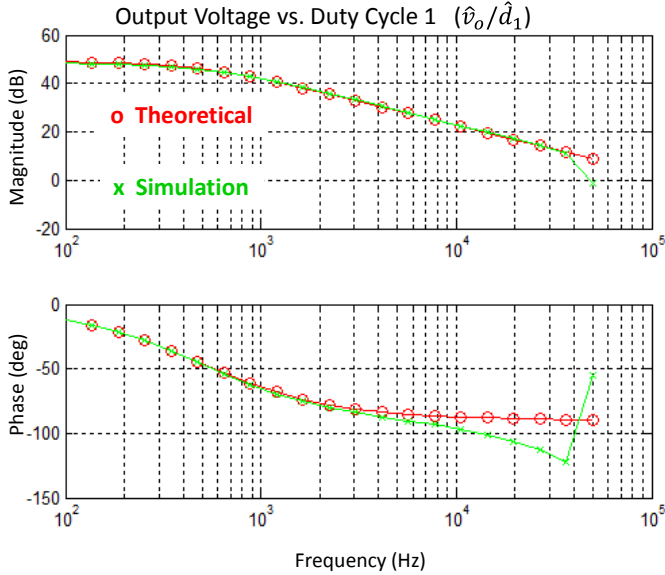


Figure 6 Bode plot of the G_{vd} obtained by calculation and through simulation

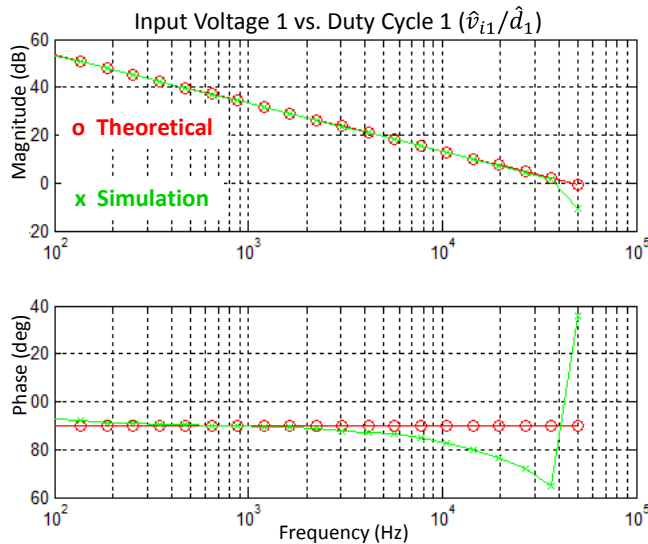


Figure 7 Bode plot of the \hat{v}_{in1}/\hat{d}_1 obtained by calculation and through simulation (simulation with PSIM)

The model has been validated by means of simulations using PSIM. The main values of the circuit parameters are: total input voltage $V_{in}=48$ V, load resistance $R=220\Omega$, switching frequency $f_{sw}=100$ kHz, inductance $L_k=6\mu H$, and transformer turns ratio $n=8$. The comparison of the theoretical and the simulated output voltage to duty cycle is shown in

Figure 6, while Figure 7 shows the input voltage to duty cycle transfer function. They exhibit a good agreement, but the phase of the simulated circuit is lower than the theoretical one at high frequencies. This is due to the time delay introduced by the modulator in the simulated circuit, which was not taken into account in the theoretical one.

B. Decoupled control loops

Differences in the input voltage of each module in steady state can appear when using a single control compensator for all the modules. In order to achieve a uniform distribution of input voltages, several strategies can be considered. One of them is to use $(K-1)$ control loops for the input voltages and an additional control loop for the output voltage, being K the number of modules. For the sake of simplicity, only three modules are considered in the calculations. The presented procedure can be easily extended to a higher number of converters.

Therefore, in the case of three modules, the controlled quantities are v_{in1} , v_{in2} and v_o (Figure 5), while the control variables are the duty cycles d_1 , d_2 and d_3 . Expressions (8) and (9) relate the controlled quantities with the control variables in the case of three modules, resulting in a MIMO (multiple input, multiple output) system.

$$\begin{bmatrix} \hat{v}_{in1} \\ \hat{v}_{in2} \\ \hat{v}_o \end{bmatrix} = \begin{bmatrix} -2A(s) & A(s) & A(s) \\ A(s) & -2A(s) & A(s) \\ Gvd(s) & Gvd(s) & Gvd(s) \end{bmatrix} \begin{bmatrix} \hat{d}_1 \\ \hat{d}_2 \\ \hat{d}_3 \end{bmatrix} = H(s) \begin{bmatrix} \hat{d}_1 \\ \hat{d}_2 \\ \hat{d}_3 \end{bmatrix} \quad (8)$$

$$A(s) = \frac{1}{3C_i \cdot s} g_{id} \quad (9)$$

The controlled quantities and control variables are very interdependent, and the conventional SISO (single input, single output) approach cannot be applied in this form. However, applying the control strategy shown in [8], the system can be manipulated in order to obtain three SISO systems.

The main idea is to define a new set of control variables (x_1 , x_2 and x_3 , (11)) in such a way that the overall system can be represented as three independent SISO systems. The strategy is to decompose the original matrix $H(s)$ as the product of two matrices, one of them diagonal. In (10) a desired diagonal matrix $D(s)$ is proposed for this particular case. Note that each element of the diagonal of $D(s)$ is a common factor of the corresponding row of the matrix $H(s)$ in (8).

$$H(s) = D(s)Y(s) = \begin{bmatrix} 3A(s) & 0 & 0 \\ 0 & 3A(s) & 0 \\ 0 & 0 & 3Gvd(s) \end{bmatrix} Y(s) \quad (10)$$

Expressions (8) and (10) can be manipulated in order to obtain a diagonal matrix that relates the controlled quantities (v_{in1} , v_{in2} and v_o) with a new set of control variables (x_1 , x_2 and x_3), as shown in (11).

$$\begin{bmatrix} \hat{v}_{in1} \\ \hat{v}_{in2} \\ \hat{v}_o \end{bmatrix} = \begin{bmatrix} 3A(s) & 0 & 0 \\ 0 & 3A(s) & 0 \\ 0 & 0 & 3G_{vd}(s) \end{bmatrix} \cdot \begin{bmatrix} \hat{x}_1 \\ \hat{x}_2 \\ \hat{x}_3 \end{bmatrix} \quad (11)$$

Expression (11) is very attractive for control loop calculations, since each controlled quantity depends only on a single control variable, and each control variable affects only to a single controlled quantity. However, a way to recover d_1 , d_2 and d_3 from the new set of control variables is required to implement physically the controller.

The relationship between the actual duty cycles and the new set of control variables is given in (12) and (13)

$$\begin{bmatrix} \hat{x}_1 \\ \hat{x}_2 \\ \hat{x}_3 \end{bmatrix} = Y(s) \begin{bmatrix} \hat{d}_1 \\ \hat{d}_2 \\ \hat{d}_3 \end{bmatrix} \quad (12)$$

$$Y^{-1}(s) = \begin{bmatrix} -1 & 0 & 1 \\ 0 & -1 & 1 \\ 1 & 1 & 1 \end{bmatrix} \quad (13)$$

Finally the true control variables d_1 , d_2 and d_3 can be calculated from x_1 , x_2 , and x_3 , according with (14).

$$\begin{bmatrix} \hat{d}_1 \\ \hat{d}_2 \\ \hat{d}_3 \end{bmatrix} = Y^{-1}(s) \cdot \begin{bmatrix} \hat{x}_1 \\ \hat{x}_2 \\ \hat{x}_3 \end{bmatrix} = \begin{bmatrix} -\hat{x}_1 + \hat{x}_3 \\ -\hat{x}_2 + \hat{x}_3 \\ \hat{x}_1 + \hat{x}_2 + \hat{x}_3 \end{bmatrix} \quad (14)$$

Once the relationship among the control variables and controlled quantities has been established in (11) and (14), the block diagram of the control system can be presented. Figure 8 shows the control loops considering the new control variables (x_1 , x_2 , and x_3). Each of the three independent control loops is composed by the plant transfer function, $3 \cdot A(s)$ and $3 \cdot G_{vd}(s)$, and the compensator transfer function $C_1(s)$ and $C_3(s)$ respectively. The compensator selection and design can be done using standard design techniques for SISO systems considering the additional gains (sensor and modulator). In this case PI compensators have been used (see section IV-C).

The output signals of the controllers in Figure 8 are the fictitious control variables x_1 , x_2 , and x_3 . Additional blocks must be added in the implemented control to recover the signals to be applied to the actual converters (d_1 , d_2 , and d_3), as shown in Figure 9.

An ideal model of the converters has been considered in the described decoupling procedure. However, the method can be applied using real models (e.g. measured frequency responses) if two conditions are met:

Condition 1: The output voltage must have the same dependence on all duty cycles (d_j) (as in (7)). Considering the case of three modules (15):

$$\left. \frac{\hat{v}_o}{\hat{d}_1} \right|_{\substack{\hat{d}_2=0 \\ \hat{d}_3=0}} = \left. \frac{\hat{v}_o}{\hat{d}_2} \right|_{\substack{\hat{d}_1=0 \\ \hat{d}_3=0}} = \left. \frac{\hat{v}_o}{\hat{d}_3} \right|_{\substack{\hat{d}_1=0 \\ \hat{d}_2=0}} \quad (15)$$

Condition 2: The transfer function of the input voltage of one module respect its own duty cycle must be proportional to the transfer function of the input voltage of the same module respect the rest of duty cycles (as in expression (6)). Considering the case of three modules (16):

$$\left. \frac{\hat{v}_{in1}}{\hat{d}_1} \right|_{\substack{\hat{d}_2=0 \\ \hat{d}_3=0}} = M \cdot \left. \frac{\hat{v}_{in1}}{\hat{d}_2} \right|_{\substack{\hat{d}_1=0 \\ \hat{d}_3=0}} = M \cdot \left. \frac{\hat{v}_{in1}}{\hat{d}_3} \right|_{\substack{\hat{d}_1=0 \\ \hat{d}_2=0}} \quad (16)$$

where M must be a constant, being in this particular case $M=-1/2$.

With these conditions, the transition matrix $Y(s)$ results in a constant coefficient matrix, as described above. Otherwise the transition matrix $Y(s)$ would include transfer functions, and the control scheme of Figure 9 would imply additional transfer functions in the recovery calculations of control variables d_j from x_j .

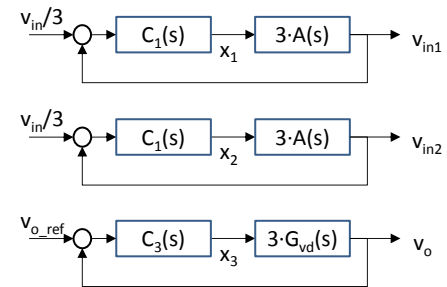


Figure 8 Block diagram considered for the calculations of the compensators

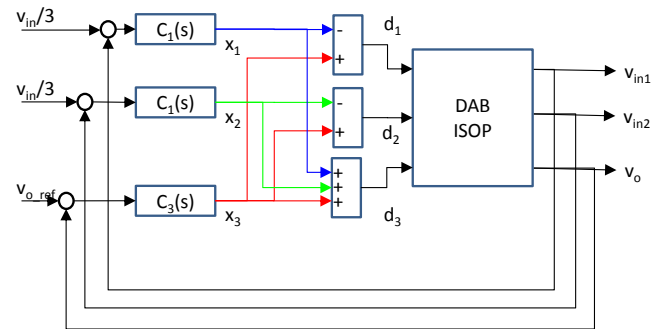


Figure 9 Block diagram considered for the implementation of the controllers

C. Effect of input capacitor mismatch

If one of the input capacitors has a different value, output voltage is not affected, but only input voltage transfer function. Based on the circuit of Figure 5, it can be derived that the input voltage transfer functions are (17) and (18), assuming that the input capacitance of module 1 is $C_{i1} = \alpha \cdot C_i$, and the other modules have an input capacitance of C_i . The relationship among (d_1 , d_2 , and d_3) and (x_1 , x_2 , and x_3) is the same that in (

14). The output transfer function G_{vd} is not affected by this variation.

$$\begin{aligned}\hat{v}_{in1} &= \frac{g_{id}}{(1+2\alpha)C_i s} \left((\hat{d}_2 + \hat{d}_3) - 2\hat{d}_1 \right) = \\ &= \frac{3}{(1+2\alpha)} 3A(s) \cdot x_1\end{aligned}\quad (17)$$

$$\begin{aligned}\hat{v}_{in2} &= \frac{g_{id}}{(1+2\alpha)C_i s} \left((\hat{d}_1 + \alpha\hat{d}_3) - (1+\alpha)\hat{d}_2 \right) = \\ &= 3A(s)x_2 + \frac{(\alpha-1)}{3} \hat{v}_{in1}\end{aligned}\quad (18)$$

If (12)-(14) are applied, the input voltage control loops can be represented as Figure 10. The control loop of input voltage 1, \hat{v}_{in1} , is affected only by a gain equal to $3/(1+2\alpha)$. The control loop of input voltage 2, \hat{v}_{in2} , is the same than in the ideal case, but with a coupling term depending on \hat{v}_{in1} . This term can be considered as a perturbation that is rejected by the control loop. For $\alpha=1.2$, which corresponds to a tolerance of 20%, the cross over frequency of \hat{v}_{in1} loop changes by a factor of 0.88 and the coupling term in the control loop of \hat{v}_{in2} is 0.067 times \hat{v}_{in1} . Therefore, the effect of input capacitor tolerance has not a great impact in the control scheme.

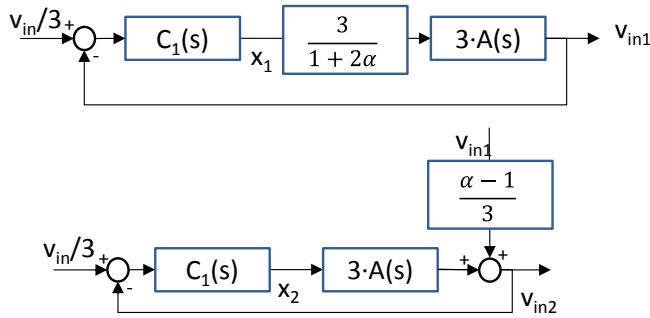


Figure 10. Input voltage control loops considering a mismatch in input capacitors value

D. Reverse (bidirectional) operation mode

The reverse operation of the proposed modular DAB converter corresponds to an IPOS (input parallel-output series) connection. The average model of this configuration is depicted in Figure 11.

The control strategy for this configuration is based on controlling the total output voltage v_o and the output voltage of (K-1) modules. In the case of three modules, the controlled quantities are v_{o1} , v_{o2} and v_o .

As the input ports of every converter are connected to an ideal voltage source, there is no interaction among them.

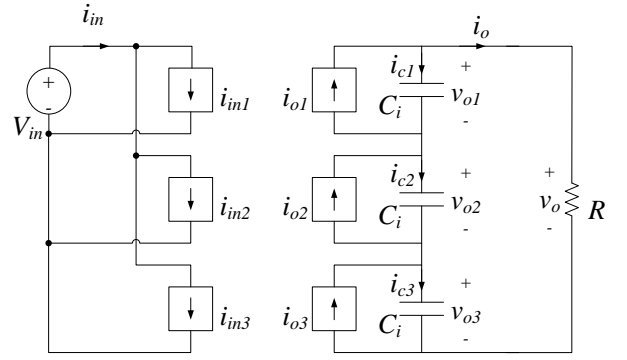


Figure 11 Bidirectional behavior of the DAB modular converter: IPOS model

Therefore, the interest is focused in the analysis of the series connected ports side.

The values of the dependent current sources in the secondary side are (19) and (20).

$$\hat{i}_{o1} = g_{od}\hat{d}_1; \hat{i}_{o2} = g_{od}\hat{d}_2; \hat{i}_{o3} = g_{od}\hat{d}_3 \quad (19)$$

$$g_{od} = \frac{TV_{in}}{L_k n} (1 - 2D) \quad (20)$$

Expression (21) relates the current and voltages at the output node of each converter.

$$\begin{aligned}\hat{i}_{o1} &= \hat{i}_o + \hat{i}_{c1} \\ \hat{v}_{o1} C_i s &= \hat{i}_{c1}\end{aligned}\quad (21)$$

Adding the equations of the three modules, the perturbation of the output current is obtained in (22):

$$3\hat{i}_o = g_{od}(\hat{d}_1 + \hat{d}_2 + \hat{d}_3) - \hat{v}_o C_i s \quad (22)$$

Considering the relationship between the output voltage v_o and the output current i_o perturbation (23), the output current is obtained in (24).

$$3\hat{i}_o = g_{od}(\hat{d}_1 + \hat{d}_2 + \hat{d}_3) - \hat{i}_o R C_i s \quad (23)$$

$$\hat{i}_o = \frac{g_{od}}{(3 + R C_i s)} (\hat{d}_1 + \hat{d}_2 + \hat{d}_3) \quad (24)$$

For the converter 1, the output voltage perturbation is expressed in (25) and (26).

$$\hat{v}_{o1} = (\hat{i}_{o1} - \hat{i}_o) \cdot \frac{1}{C_i s} \quad (25)$$

$$\hat{v}_{o1} = \frac{g_{od}}{C_i s} \cdot \hat{d}_1 - \frac{g_{od}}{C_i s} \cdot \frac{1}{(3 + R C_i s)} (\hat{d}_1 + \hat{d}_2 + \hat{d}_3) \quad (26)$$

The total output voltage perturbation is:

$$\hat{v}_o = \frac{g_{od}R}{(3 + RC_i s)} \cdot (\hat{d}_1 + \hat{d}_2 + \hat{d}_3) = Gvd_2(s)(\hat{d}_1 + \hat{d}_2 + \hat{d}_3) \quad (27)$$

Therefore, the model of the modular converter in IPOS connection is expressed in (28) and (29).

$$\begin{bmatrix} \hat{v}_{o1} \\ \hat{v}_{o2} \\ \hat{v}_o \end{bmatrix} = \begin{bmatrix} A_2(s) & A_2(s)A_3(s) & A_2(s)A_3(s) \\ A_2(s)A_3(s) & A_2(s) & A_2(s)A_3(s) \\ Gvd_2(s) & Gvd_2(s) & Gvd_2(s) \end{bmatrix} \begin{bmatrix} \hat{d}_1 \\ \hat{d}_2 \\ \hat{d}_3 \end{bmatrix} = H_2(s) \begin{bmatrix} \hat{d}_1 \\ \hat{d}_2 \\ \hat{d}_3 \end{bmatrix} \quad (28)$$

$$A_2(s) = \frac{g_{od}}{C_i s} \cdot \frac{2 + RC_i s}{3 + RC_i s}; \quad A_3(s) = \frac{-1}{2 + RC_i s} \quad (29)$$

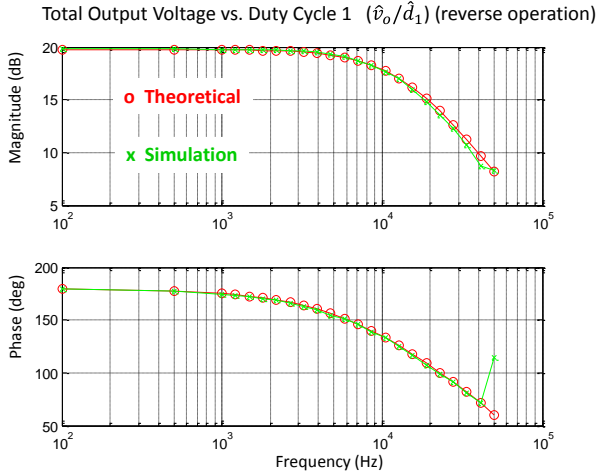


Figure 12 Bode plot of the \hat{v}_o/\hat{d}_1 obtained by calculation and through simulation (simulation with PSIM)

Comparison between theoretical and simulation results are shown in Figure 12, Figure 13 and Figure 14. In this case the decoupling strategy cannot be strictly applied like in the case of ISOP configuration, since condition II (16) is not met. However, the analysis of $A_3(s)$ in (29) can provide design criteria. If the frequency range considered for the control design is lower than the frequency of the pole of $A_3(s)$, this term can be considered as a constant (30) and then the control strategy proposed in the previous section can be applied.

$$A_3(s) \approx \frac{-1}{2} \text{ if } s = j\omega \text{ and } \omega \ll \frac{2}{RC_i} \quad (30)$$

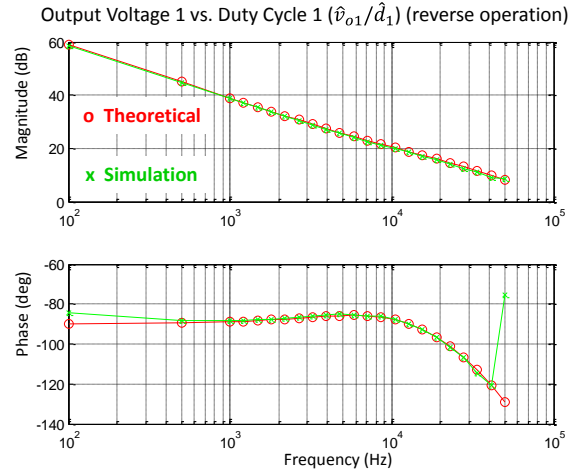


Figure 13 Bode plot of the \hat{v}_{o1}/\hat{d}_1 obtained by calculation and through simulation (simulation with PSIM: dashed line; theoretical: solid line)

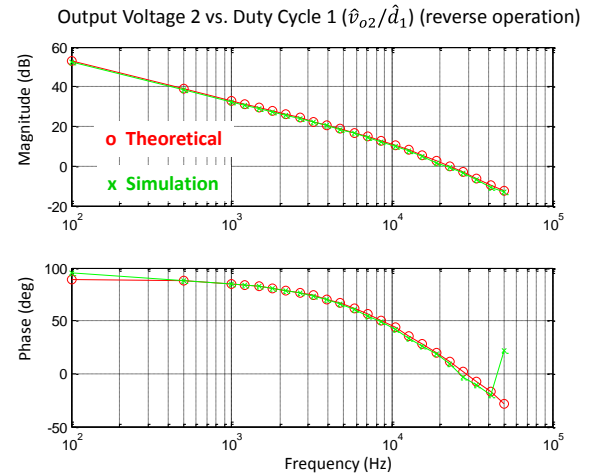


Figure 14 Bode plot of the \hat{v}_{o2}/\hat{d}_1 obtained by calculation and through simulation (simulation with PSIM)

IV. EXPERIMENTAL RESULTS

A modular DAB converter with 3 modules has been designed and built in order to test the control approach presented in this paper. The main characteristics of the modular converter are summarized in Table 1, and the experimental setup is shown in Figure 15. The control stage has been implemented with an FPGA and three ADC (analog to digital converters), and it includes a modulator for each module (generation of control pulses) and compensators, allowing open loop or closed loop operation. The use of an FPGA is justified in this case by the high number of control signals to be generated. Although the control can be implemented with analog circuitry, the FPGA provides flexibility for prototype testing.

Table 1 Characteristics of the modular converter

Nominal Total input voltage V_{in}	100 V	Nominal output voltage V_o	250 V
Input capacitance (per module)	490 μ F	Output capacitance (per module)	1.5 μ F
Inductance L_k	3.6 μ H (nominal)	Load minimum resistance R	67 Ω
Switching frequency	100 kHz	Transformation ratio n	1:7 (nominal)

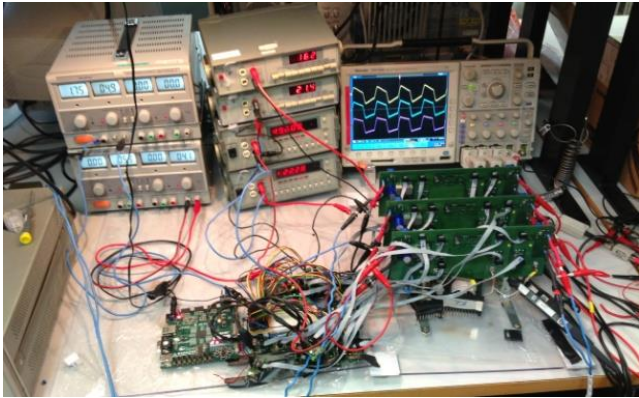


Figure 15 Picture of the experimental prototype of three DAB converter in ISOP connection

A. Input voltage mismatch illustration (open loop operation)

In order to illustrate the influence of different parameters in the input voltage distribution for the DAB with ISOP connection, the measured input voltage distribution in steady state is shown in Figure 16 and Figure 17. These results correspond to the actual prototype where components are intended to be equal among the modules (leakage inductance, transformation ratio, effective duty cycle, etc), but their actual values exhibit some dispersion due to the tolerance of components.

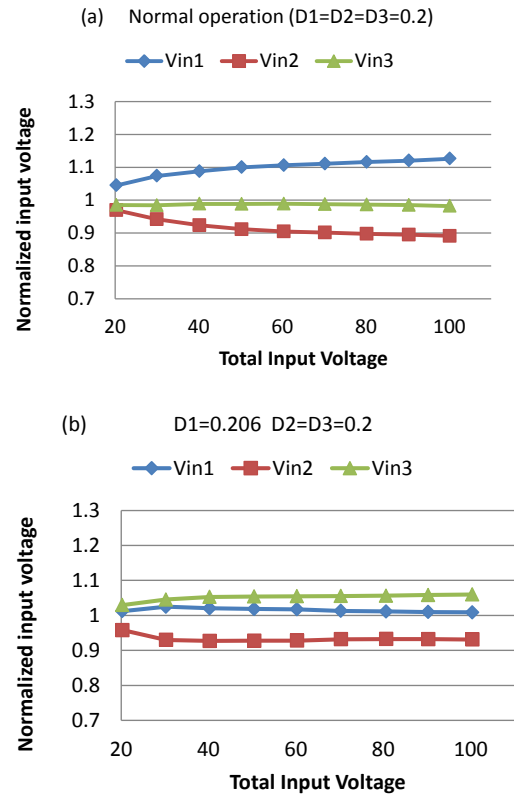


Figure 16 Input voltage distribution in an actual prototype with 3 modules. a) All duty cycles have the same value b) Increasing of duty cycle has been applied in module 2. c) Duty cycle distribution is modified to compensate module differences.

The plot in Figure 16 represents the input voltage of each module (v_{in1} , v_{in2} and v_{in3}) normalized to the ideal value (one third of the total input voltage) versus the total input voltage, with $R=80 \Omega$. In Figure 16a) the three duty cycles $D1$, $D2$ and $D3$ have been set to the same value. Note that the higher the input voltage, the higher the relative difference in the input voltage. However, the trend is to achieve a constant relative difference although the total input voltage increases. In Figure 16b) a slight variation of the duty cycle of one module has been applied in order to compensate the deviation from the average of the input voltages. In this case, $D1$ has been changed to compensate the dispersion of other values (leakage inductance, transformer voltage ratio, etc.)

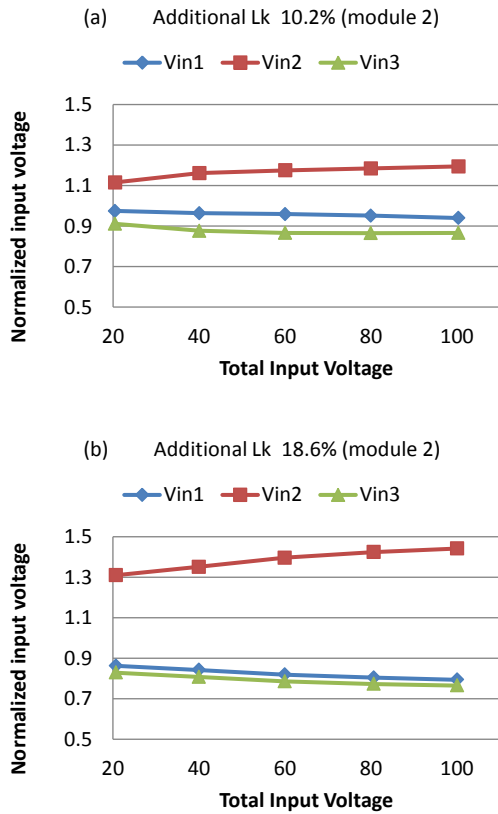


Figure 17 Input voltage distribution in an actual prototype with 3 modules. All modules have the same duty cycle $D=0.2$. a) An additional leakage inductance equals to 10,2 % of the nominal value has been added in module 2. b) An additional leakage inductance equals to 18.6% has been added in module 2.

The influence of the leakage inductance is illustrated in Figure 17. The leakage inductance of module 2, which in the implemented prototype is an additional physical component, has been increased by adding a new ferrite core to the wire that connects the inductor to the PCB. If an additional leakage inductance of 10.2% of the nominal value is added in module 2, the input voltage distribution changes (Figure 17a), compared to the initial situation (Figure 16a). Module 2 has now the higher voltage of the three modules in all the input voltage range, and the difference among the input voltages is higher: +19.4%, -13.4%. If an additional leakage inductance equals to 18.6% of the nominal value is added to module 2, Figure 17b), the input voltage distribution has the same trend: module 2 has the higher input voltage (+44.1%) while module 3 is lower voltage (-24.5%).

These experiments illustrate the issue of voltage distribution in series connected DAB converters. Since the input voltage distribution depends on the random dispersion of the value of some elements, control loops over the input voltages should be used to ensure a proper input voltage sharing.

B. Verification of the model

In order to assess the applicability of the described control strategy to an actual prototype, frequency response of the DAB converters in ISOP connection (forward operation mode) has been measured with a frequency response analyzer (FRA). The prototype of Figure 15 is controlled by the FPGA in open loop. Control pulses for modules 2 and 3 are generated with a fixed duty cycle, while the duty cycle of module 1 is perturbed by adding the signal generated by the FRA oscillator to an offset voltage.

Output voltage to duty cycle response (\hat{v}_o/\hat{d}_1) is shown in Figure 18. This response is a first order system with an additional delay (phase loss) due to the modulator. The measurement result has been corrected taking into account the attenuation of the probes, the gain introduced by the ADC and modulator (58 dB of overall attenuation). A time delay equal to 5 μ s has been taken into account in the model computation. Measurements agree with the model over a wide frequency range.

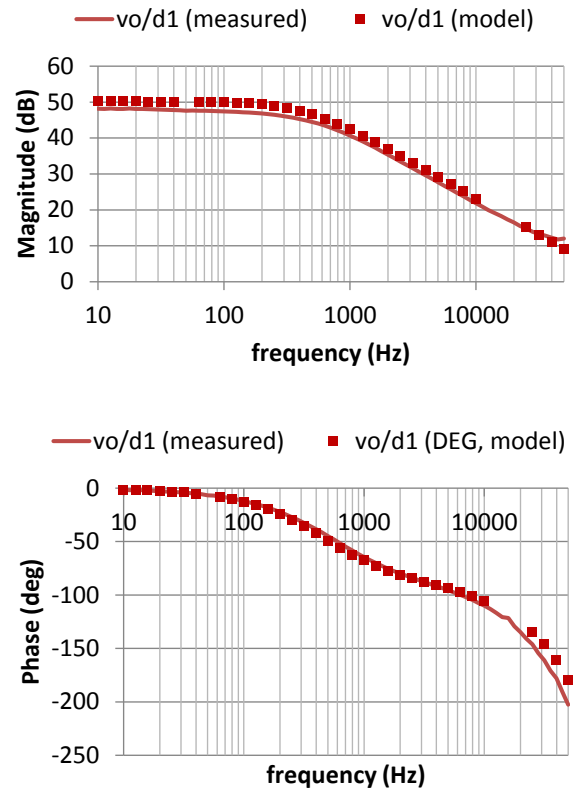


Figure 18 Frequency response of the actual prototype. Output voltage to duty cycle transfer function.

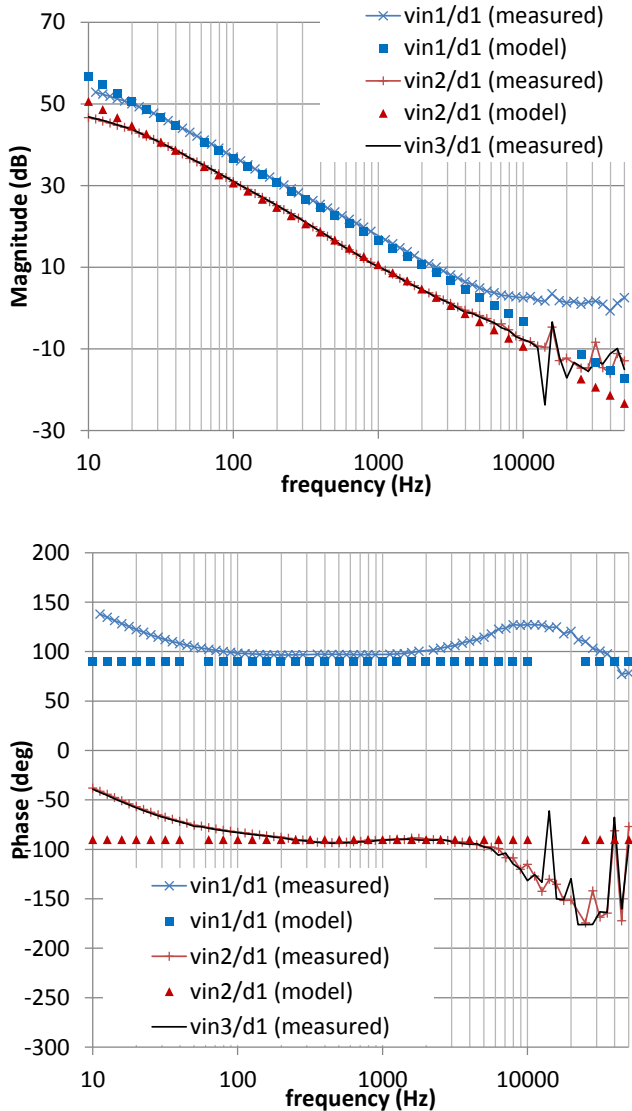


Figure 19 Input voltage to duty cycle transfer functions.

Moreover, variations of the input voltages of each module have also been measured, with the same setup. In this case the focus is on the transfer function of the input voltage to duty cycle (\hat{v}_{in}/\hat{d}_1). The described control approach assumes that the transfer function of input voltage to its own duty cycle must be proportional to the transfer function of input voltage to other duty cycle (16). In order to validate this condition, duty cycle of module 1 has been perturbed. Figure 19 shows the amplitude and phase plot of the transfer function, where a constant difference of 6 dB in magnitude and 180° in phase is obtained in a relatively wide frequency range (up to 5 kHz) and therefore the decoupling loop technique can be applied. In this case, it is more important the relative difference among the input voltage transfer functions than the perfect match with the theoretical model. Transfer functions have been measured for a

total input voltage of 100 V, $R=80 \Omega$, and nominal D equal to 0.2.

C. Proposed control strategy validation (closed loop operation)

In this paper, experimental verification of the proposed control strategy applied to the modular DAB converter is reported.

PI controllers have been used as compensator (C1(s) and C3(s) in Figure 8 and Figure 9). They have been described in VHDL and adjusted specifically for this experimental setup. The control law has been implemented by the difference equation (31).

$$x_k = Ge \cdot e_k + Ge1 \cdot e_{k-1} + x_{k-1} \quad (31)$$

Where e_k and e_{k-1} are the samples of the error signal, and x_{k-1} is the last value of the control signal. Ge and Ge-1 are the coefficients of the compensator. For the input voltage control loops, $Ge=0.06097412109375$ and $Ge1=-0.060958$ with sampling period of 5 μs and overall constants (ADC, modulator and sensor) $K=0.0045$. In the case of the output voltage control loop, $Ge=0.6181640625$ and $Ge1=-0.58984375$, with the same sampling period and overall constants $Ko=5.0967e-4$. Compensators have been adjusted to obtain a cross over frequency equal to 4 Hz for the input voltage control loops and 200 Hz for the output voltage control loop.

In order to show the suitability of the control strategy, intentional mismatch among the modules has been induced, modifying the leakage inductance in module 2, as explained before. This causes a difference among the modules in such a way that with identical duty cycles the conversion ratio for each module is different, and then the input voltage distribution is not uniform. This distribution should be uniform using the proposed control strategy.

Results corresponding to an output power value of 950 W are presented in Figure 20. In Figure 20a) the input voltages with no additional component in the modules are shown. Only the output voltage is controlled and all modules receive the same control signal. In this case, the maximum difference is found at the lower input voltage. While module 1 has 117.5% of the ideal input voltage, module 2 has 84.7% of the ideal input voltage.

The results with an additional inductance (370 nH, i.e., 10.2% the nominal value) in module 2 are shown in Figure 20b). In this case, the difference becomes higher: module 2 has 154.5% of the ideal input voltage and module 3 has only 64.7% of the ideal input voltage.

The results obtained using the proposed control approach with additional control loop for v_{in} are shown in Figure 20c). In this case, module 2 has also an additional leakage inductance equal to 370 nH. The maximum relative difference is 5.3% for module 3. Additional tests for a lower power and a higher

additional inductance shows also a good distribution of the input voltages, with a relative difference lower than $\pm 2\%$.

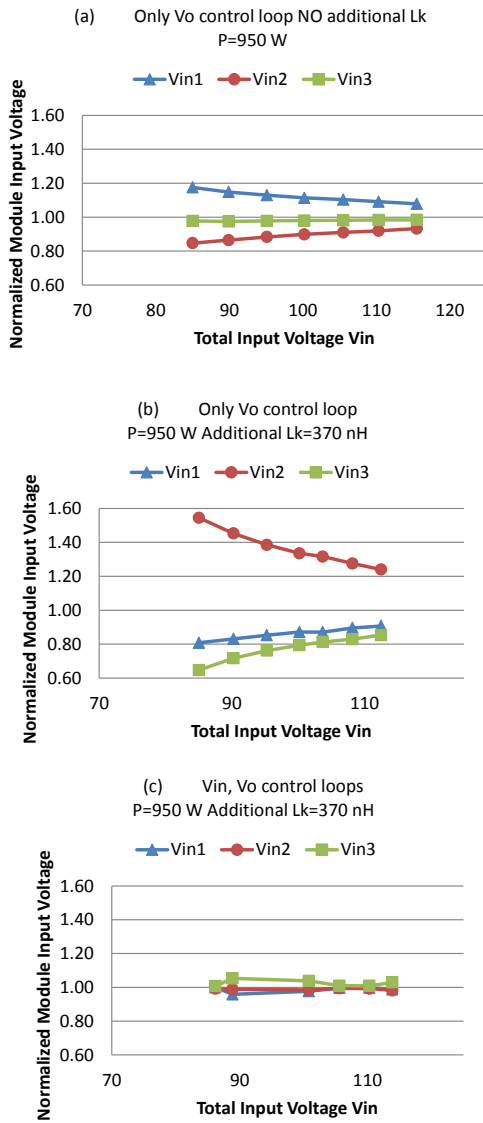


Figure 20 Input voltage distribution for single control loop of the output voltage (Only V_o control) and the proposed control strategy (V_{in}, V_o control loops). a) No modification on the modules, control of V_o . b) Additional L_k in module 2, control of V_o . c) Proposed control strategy (control of V_{in} and V_o) with additional L_k in module 2.

Loop gains have been measured, in order to compare with expected theoretical predictions. In Figure 21 the measured open loop gains are shown for $V_{in}=100$ V, $V_o=250$ V and $R=67\Omega$. The theoretical response has been obtained using the model measurements and the theoretical compensator response. Note that measurements have been taken with the three control loops in operation. The low frequency response is difficult to measure due to the limitation of the injection transformer used in the measurement setup. In the range where the measurement is valid, expected results match the experimental data.

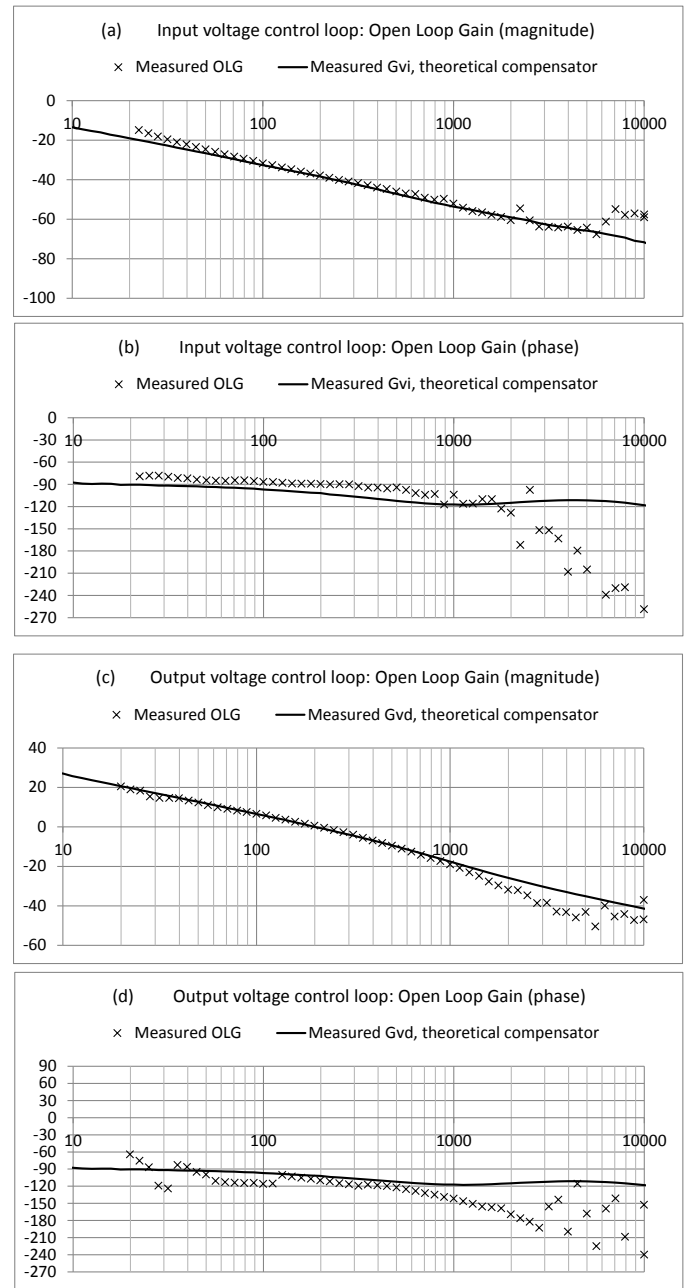


Figure 21 Measured vs. theoretical open loop gain for input voltage loop (a and b) and for output voltage loop (c and d)

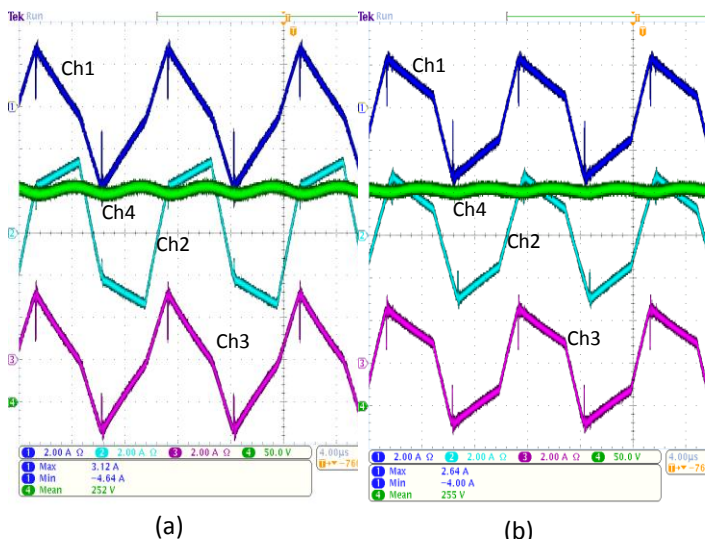


Figure 22 Waveforms of inductor currents (I_{Lk}) with an additional leakage inductance in one module. a) Only the output voltage is controlled and all modules share the same duty cycle. b) Proposed control loop strategy. Channel 1: I_{Lk} Module 1, Channel 2: I_{Lk} Module 2, Channel 3: I_{Lk} Module 3 and Channel 4: output voltage

In order to illustrate one of the effects of non-uniform voltage distribution two tests have been carried out in the following conditions: the input voltage is 80 V, the output voltage is 250 V, the output power is 800 W and module 2 has an additional leakage inductance of 670 nH.

In the first test, controlling only the output voltage and applying the same duty cycle to all modules, a non uniform distribution of the input voltages is obtained ($V_{in1}=14.88$ V, $V_{in2}=50.6$ V and $V_{in3}=14.68$ V) as expected. The waveforms of the current through the leakage inductance are shown in Figure 22a), where module 1 and module 3 are near from losing the ZVS condition[22], due to the values of the inductor current in the switching instant .

In the second test the proposed control strategy is applied to the three modules, obtaining a more uniform input voltage distribution ($V_{in1}=26.6$ V, $V_{in2}=26.3$ V and $V_{in3}=27.04$ V). In this case, the waveforms of current through the leakage inductance (Figure 22b)) are similar. In this case the ZVS condition is clearly met for all modules.

V. CONCLUSIONS

A modular architecture based on DAB converters in ISOP connection has been studied in this paper. One of the main concerns in ISOP modular architectures is a proper input voltage sharing among the DAB modules, since small differences among each module can result in large differences in the input voltages distribution. Therefore, the control strategy must ensure a proper distribution of input voltages in order to: 1) ensure that all the modules process the same power and it is not necessary to overrate them; 2) guarantee ZVS condition of each module in a wide range of operation (especially in the case of DAB modules using PSM).

A small signal model of the modular DAB converter has been derived from the model of a single module. Considering the modular converter from an external point of view, it behaves like a single converter controlled by the addition of the control signal of all modules. However, from an internal point of view, the input voltage of each converter depends in a different way on its own control signal that on the rest of control signals. Therefore, the regulation of the input voltages and output voltage depends on all duty cycles at the same time.

In order to decouple the control loop, a classical control scheme oriented to the ISOP architecture has been applied to control the output voltage and the input voltages. Applying a technique of decoupling control loops, based on combining the output signal of the compensators, a much simpler control scheme is obtained.

The proposal has been tested on a laboratory prototype. The model of the modular system has been validated by measuring the small-signal functions while operating open-loop. Then the proposed control strategy has been implemented and tested. On one hand, open loop gains have been measured. On the other hand, steady state measurements have been performed varying the total input voltage, considering different load levels and modifying the leakage inductance of one module to illustrate the component value dispersion. The results show that the distribution of the input voltages is uniform for various operating conditions and for different values of the constructive parameters of the modules.

ACKNOWLEDGEMENTS

This work was supported by the Spanish Ministry of Science and Innovation under the coordinate project FLAME and the subprojects ARQUIFLAME (DPI2010-21110-C02-01) and MODUFLAME (DPI2010-21110-C02-02), and also by the Secretaria Nacional de Educación Superior, Ciencia, Tecnología e Innovación del Ecuador (SENESCYT).

REFERENCES

- [1] G. Gong, D. Hassler, J. W. Kolar, "A Comparative Study of Multicell Amplifiers for AC-Power-Source Applications", IEEE Transactions on Power Electronics, vol. 26, no. 11, Jan. 2011
- [2] R. Ayyanar, R. Giri, N. Mohan "Active Input-Voltage and Load-Current Sharing in Input-Series and Output-Parallel Connected Modular DC-DC Converters Using Dynamic Input-Voltage Reference Scheme", IEEE Transactions on Power Electronics, vol. 19, no. 6, pp. 1462-1473, Nov. 2004
- [3] J. Song-Manguelle, M. H. Todorovic, "A Modular Stacked DC Transmission and Distribution System for Long Distance Subsea Applications", IEEE Transactions on Industry Applications, vol. 50, no. 5, Sep./Oct. 2014
- [4] J.-W. Kim; J.-S. Yon; B.-H. Cho, "Modeling, Control, and Design of Input-Series-Output-Parallel-Connected Converter for High-Speed-Train Power System," IEEE Transactions on Industrial Electronics, vol.48, no.3, pp.536-544, Jun. 2001
- [5] Q. Ting, B. Lehman, "Coupled Input-Series and Output-Parallel Dual Interleaved Flyback Converter for High Input Voltage Application", IEEE Transactions on Power Electronics, vol. 23, no. 1, pp. 88-95, Jan. 2008

- [6] T. Jin, K. Zhang, K. Zhang, K. Smedley, "A New Interleaved Series Input Parallel Output (ISIPO) Forward Converter With Inherent Demagnetizing Features", *IEEE Transactions on Power Electronics*, vol. 23, no. 2, pp. 888-895, Mar. 2008
- [7] V. Choudhary, E. Ledezma, R. Ayyanar, R. M. Button, "Fault Tolerant Circuit Topology and Control Method for Input-Series and Output-Parallel Modular DC-DC Converters", *IEEE Transactions on Power Electronics*, vol. 23, no. 1, pp. 402-411, Jan. 2008
- [8] X. Ruan, W. Chen, L. Cheng, C. Tse, Hong Yan, Tao Zhang, "Control Strategy for Input-Series-Output-Parallel Converters", *IEEE Transactions on Industrial Electronics*, vol. 56, no. 4, Apr. 2009
- [9] R. W. DeDoncker, D.M. Divan, M.H. Kheraluwala, "A Three-Phase Soft-Switched High Power-Sensity DC/DC Converter for High Power Applications", *IEEE Transactions on Industry Applications*, vol. 27, pp. 63-73, Jan. 1991
- [10] M. H. Kheraluwala, R. W. Gascoigne, D. M. Divan, E.D. Baumann, "Performance Characterization of a High-Power Dual Active Bridge DC-TO-DC Converter", *IEEE Transactions on Industry Applications*, vol. 28, pp. 1294-1301, Nov. 1992
- [11] F. Krismer, J. W. Kolar, "Accurate Power Loss Model Derivation of a High-Current Dual Active Bridge Converter for an Automotive Application", *IEEE Transactions on Industrial Electronics*, vol. 57, no. 3, Mar. 2010
- [12] F. Krismer, S. Round, J. W. Kolar, "Performance Optimization of a High Current Dual Active Bridge with a Wide Operating Voltage Range", *IEEE Power Electronics Specialists Conference (PESC)*, pp.1-7, Jun. 2006
- [13] F. Krismer, J.W. Kolar, "Accurate Small-Signal Model for the Digital Control of an Automotive Bidirectional Dual Active Bridge", *IEEE Transactions on Power Electronics*, vol. 24, no. 12, Dec. 2009
- [14] F. Krismer, J. W. Kolar, "Closed Form Solution for Minimum Conduction Loss Modulation of DAB Converters," *IEEE Transactions on Power Electronics*, vol. 27, no. 1, pp. 174-188, Jan. 2012
- [15] F. Krismer, J. W. Kolar, "Efficiency-Optimized High-Current Dual Active Bridge Converter for Automotive Applications", *IEEE Transactions on Industrial Electronics*, vol. 59, no. 7, pp. 2745-2760, Jul. 2012
- [16] A. K. Tripathi, K. Mainali, D. C. Patel, A. Kadavelugu, S. Hazra, S. Bhattacharya, et al., "Design Considerations of a 15-kV SiC IGBT-Based Medium-Voltage High-Frequency Isolated DC-DC Converter," *Industry Applications*, *IEEE Transactions on*, vol. 51, pp. 3284-3294, 2015.
- [17] B. S. Poshtkouhi and O. Trescases, "Flyback Mode for Improved Low-Power Efficiency in the Dual-Active-Bridge Converter for Bidirectional PV Microinverters With Integrated PV Storage," *Industry Applications*, *IEEE Transactions on*, vol. 51, pp. 3316-3324, 2015.
- [18] C. B. Farhangi and H. A. Toliyat, "Piecewise Linear Model for Snubberless Dual Active Bridge Commutation," *Industry Applications*, *IEEE Transactions on*, vol. 51, pp. 4072-4078, 2015
- [19] T. Hirose, M. Takasaki, "A Power Efficiency Improvement Technique for a Bidirectional Dual Active Bridge DC-DC Converter at Light Load", *IEEE Transactions on Industry Applications*, vol. 50, no. 6, Nov./Dec. 2014
- [20] H. Akagi, T. Yamagishi, N. M. L. Tan, S. -I. Kinouchi, Y. Miyazaki, M. Koyama, "Power-Loss Breakdown of a 750 V 100 kW 20 kHz Bidirectional Isolated DC-DC Converter Using SiC-MOSFET/SBD Dual Modules", *IEEE Transactions on Industry Applications*, vol. 51, no. 1, pp.420-428, Jan./Feb. 2015
- [21] A.R. Alonso, J. Sebastian, D.G. Lamar, M.M. Hernando, A. Vazquez, "An Overall Study of a Dual Active Bridge for Bidirectional DC/DC Conversion", *IEEE Energy Conversion Congress and Exposition (ECCE)*, pp. 1129-1135, Sept. 2010
- [22] A. Rodriguez, A. Vazquez, D. G. Lamar, M. M. Hernando, J. Sebastian, "Different Purpose Design Strategies and Techniques to Improve the Performance of a Dual Active Bridge with Phase-Shift Control", *IEEE Transactions on Power Electronics*, vol. 30, no. 2, pp. 790-804, Feb. 2015
- [23] R.T. Naayagi, A.J. Forsyth, R. Shuttleworth, "Bidirectional Control of a Dual Active Bridge DC-DC Converter for Aerospace Applications", *IET Power Electronics*, 2012, Vol. 5, Iss. 7, pp. 1104-1118
- [24] G. Ortiz, J. Biela, D. Bortis, J. W. Kolar, "1 MegaWatt, 20 kHz, Isolated, Bidirectional 12kV to 1.2kV DC-DC Converter for Renewable Energy Applications", *International Power Electronics Conference (IPEC)*, 2010
- [25] H. Zhou, A. Khambadkone, "Hybrid Modulation for Dual-Active-Bridge Bidirectional Converter with Extended Power Range for Ultracapacitor Application", *IEEE Transactions on Industry Applications*, vol. 45, no. 4, Jul./Aug. 2009
- [26] J. W. Kolar, T. Friedli, F. Krismer, A. Looser, M. Schweizer "Conceptualization and Multi-Objective Optimization of the Electric System of an Airborne Wind Turbine", *IEEE International Symposium on Industrial Electronics (ISIE)*, 2011
- [27] P. Zumel, L. Ortega, A. Lazaro, C. Fernandez, A. Barrado, "Control Strategy for Modular Dual Active Bridge Input Series Output Parallel," *IEEE 14th Workshop on Control and Modeling for Power Electronics (COMPEL)*, pp. 1-7, Jun. 2013